Egypt. J. Chem. **Vol. 66**, No. SI: 13 pp. 483 - 497 (2023)

Egyptian Journal of Chemistry

http://ejchem.journals.ekb.eg/

Electronic Structure, Spectra and Chemical Reactivity Descriptors of Some Novel Rhodanine Derivatives. Density Functional Theory Approach

Mahmoud Sharaf,[a] H. Moustafa,[a*] Rifaat H. Hilal[a]

[a]*Chemistry Department, Faculty of Science, Cairo University, University Ave., Dokki, Cairo 12613, Egypt*

Abstract

The ground state optimized structure of the newly synthesized and characterized **2-4** rhodanines derivatives were investigated theoretically at the B3LYP/6-311++G** level of theory. The optimized structure is planar with the N-ph. moiety out of the molecular plane by 90^0. The correspondence between the theoretically computed and x-ray experimentally measured geometric parameters is excellent. The electronic absorption spectra of the rhodanines **1**-**5** are measured in both polar and nonpolar solvents. Assignments of the experimentally recorded transitions are facilitated via computation of the spectra at the TD-DFT/B3LYP/6-311++G** level of theory. Natural transition orbitals (NTO) enable deep insight into the nature of the observed electronic transitions. Gross Solvents effects are cogitated by applying Polarizable Continuum Model (PCM) in the TD-DFT computations. Compounds **2-5** displayed the two π-π* rhodanine ring transitions at 294 nm and 252 nm besides a new band due to 5-arylmethylidene group in position 5 for Rh ring. The computed HOMO - LUMO energies of the investigated compounds could be utilized to determine the overall characteristics parameters. The order of increasing E_{HOMO} is **3** < **1** < **5** < **2** < **4** while the order of decreasing E_{LUMO} is **3** < **5** < **2** < **4** < **1**. From these results it is obvious that derivative **4** holds the uppermost nucleophilicity while compound **3** has the highest electrophilicity. Analyzing the computed hardness (η) values and softness (S) values for the studied compounds revealed their donor-acceptor behavior, Results of the present work indicate that compound **4** is the most polarizable, of the highest chemical reactivity and easier charge transfer with S=0.3117 eV, while the least is compound **1** with η=2.1722 eV. The molecular electrostatic potential (MEP) maps are correlated to the electronic density and are a highly useful signifier for elucidating electrophilic and nucleophilic reaction sites, as well as hydrogen bonding interactions and chemical activity. Negative areas are mostly gone over O7 atom of CO group for compounds (**1-5**) and the nitrogen atoms of pyridine group for compound **3**, while S6 atom in compound **4** is slightly red. These are the molecular residues that are most frequently targeted by electrophilic attacks.

Keyword: Rhodanine derivatives; Density Functional Theory (DFT); UV spectra; NTO analysis; Global descriptors

1. Introduction

Rhodanine compounds as heterocyclic Oxygen, nitrogen and sulfur conveying five membered rings in the discovery and promotion of drugs became an important class of structures for deep survey. [1]. The clinical trials for numerous type of diseases such as neuropathy, nephropathy and cataract diabetic complications (insulin sensitizing), type II diabetes mellitus, together with antitumor behaviors, aldose reductase inhibitor, and pancreatic cholesterol esterase inhibition are made by these class of molecules [2]. To achieve the capacious spectrum pharmacological activity modification of thiazolidine-4-one (rhodanine ring) on positions 5, 4, 3 or 2 used successfully to attain the chemically desired synthesized materials.

The medicinal Perspective of Thiazolidinones: is the subject of several reviews [3,4] whilst its antioxidant and/or anti-inflammatory properties are reported [5,6]. Rhodanines was shown to be Potential Anti-Bacterial Agents [7], and have antimicrobial and antitubercular activity [8–10]. A critical review about

*Corresponding author e-mail: husseinmam@hotmail.com.;(H. Moustafa)
EJCHEM use only: Received date 28 February 2023; revised date 03 April 2023; accepted date 12 April 2023
DOI: 10.21608/EJCHEM.2023.196920.7651

the utility of rhodanines as a Scaffold in Drug Discovery is published by Tomašić [11].

conceivably reactive and electrophilic substances 5-arylmethylidenerhodanines -by reason of feasible Michael addition of nucleophilic residues of the protein to their double bond (exocyclic) - are forming The vast majority of rhodanines that are biologically active. [12,13].

Numerous pharmacological effects of rhodanines encompass antidiabetic, bacterial, fungal resistance, anti-infective, pesticidal, as well as antimycobacterial, antineoplastic, antitubercular, anti-inflammatory, anti-human immunodeficiency virus (HIV), antioxidant and antimalarial effects. [14–16].

The present study aims to introduce novel rhodanine derivatives and pinpoint those, structure properties, global reactivity descriptors, and spectral features in the UV-Vis regions using polar and nonpolar solvents, which underlay their biological properties. The following objectives will be addressed; investigate theoreti□ally the ground state properties of researched rhodanine **1-5** products utilizing B3LYP/6-311++G(d,p) level of theory. Descriptors of the examined rhodanines **1-5** , such as hardness (η), electronegativity (χ), and softness (S) will be calculated and considered. Experimental measurement and theoretical electronic spectrum computations in the UV region of the derivatized rhodanines **1-5** utilizing time dependent density functional theory TD-DFT and nature transition orbitals(NTO) will be done employing 6-311++G (d, p) basis sets. Interpretation of each absorption band's origin, furthermore to the molecular orbitals (MOs) and contributing configurations, are described, and analyzed. HOMO-LOMO maps of all orbitals involved in the vertical transitions of the studied rhodanine **1-5** derivatives are valuable assessments that may be utilized to visualize the variously charged areas of a molecule and illuminate the charge distributions of molecules.

2. Experimental

2.1. Synthesis

Compound 1, **3-phenyl-2-thioxothiazolidin-4-one**

starting moiety (**1**) for preparation of the investigated compounds, was prepared according to previously published method sited in [18]. The newly synthesized compounds (**2-5**) were prepared using the following routine, 3-Phenyl-2-thioxothiazolidin-4-one (10.5 g, 50 mmol) was dissolved in glacial acetic (50 ml). To the resulting solution, the appropriate aldehyde (50 mmol) with sodium acetate (12 g) were introduced, and the combination refluxed for 1 hr. The precipitated product crystallized after filtering from acetic acid to give the corresponding 5-arylmethylidene-3-phenyl-2-thioxothiazolidin-4-one listed in Supplementary Table 1.

3-phenyl-5-(thiophen-2-ylmethylene)-2-thioxothiazolidin-4-one

Yellow crystals; mp 202-204 ˚C (DMF + ETOH); yield 69%; IR (νmax, cm-1) ν 1706 (C=O) ; 1H NMR (300 MHz , DMSO-d6) δ 7.33-7.57 (m, 6H, Ar-H), 7.79 (S, 1H, =C-H) and 8.11-8.14 (m, 2H, Ar-H); 13C NMR (75 MHz, DMSO-d6) δ 120.40, 120.58, 125.85, 128.74, 129.30, 129.45, 134.78, 135.30, 135.89, 137.45, 166.65 and 192.93. Anal. Calcd. for C14H9NS3O (303.41): C, 55.42; H, 2.99; N, 4.62; S, 31.70. found C, 55.49; H, 2.93; N, 4.68; S, 31.81.

3-phenyl-5-(pyridin-4-ylmethylene)-2-thioxothiazolidin-4-one (3)

Yellow crystals; mp 235-237 ˚C (DMF); yield 72%; IR (νmax, cm-1) ν 1712 (C=O) ; 1H NMR (300 MHz , DMSO-d6) δ 7.42-7.61 (m, 7H, Ar-H), 7.79 (S, 1H, =C-H) and 8.75 (d, 2H, 2 N-C-H); 13C NMR (75 MHz, DMSO-d6) δ 123.67, 128.44, 128.69, 129.11, 129.36, 129.57, 134.97, 139.97, 150.74, 166.68 and 192.93. Anal. Calcd. for C15H11N2S2O (298.38): C, 60.38; H, 3.38; N, 9.39; S, 21.49. found C, 60.40; H, 3.34; N, 9.42; S, 31.94.

5-(Benzo[d][1,3]dioxol-5-ylmethylene)-3-phenyl-2-thioxothiazolidin-4-one (4)

Yellow crystals; mp 199-200˚C (DMF); yield 76%; IR (νmax, cm-1) ν 1705 (C=O) ; 1H NMR (300 MHz , DMSO-d6) δ 6.16 (s, 2H, O-CH2-O), 7.12 (m, 8H, Ar-H) and 7.77 (s, 1H, =C-H); 13C NMR (75 MHz, DMSO-d6) δ 102.21, 109.38, 109.69, 120.57, 126.93, 127.26, 128.71, 129.29, 129.40, 132.94, 135.24, 148.37, 149.85, 166.95 and 193.62. Anal. Calcd. for C17H11NS2O3 (341.40): C, 59.80; H, 3.25; N, 4.10; S, 18.78. found C, 59.96; H, 3.34; N, 4.03; S, 18.82.

5-(4-Fluorobenzylidene)-3-phenyl-2-thioxothiazolidin-4-one (5)

Yellow crystals; mp 220-222˚C (DMF); yield 79%; IR (νmax, cm-1) ν 1711 (C=O) ; 1H NMR (300 MHz , DMSO-d6) δ 7.37-7.77 (m, 9H, Ar-H) and 7.85 (s, 1H, =C-H); 13C NMR (75 MHz, DMSO-d6) δ 116.90, 122.96, 128.71, 129.32, 129.46, 131.52, 133.20, 135.14, 161.48, 164.82, 166.90 and 193.79. Anal. Calcd. for C17H11NS2O3 (315.38): C, 60.93; H, 3.20; F, 6.02; N, 4.44; S, 20.33. found C, 60.85; H, 3.18; F, 5.95; N, 4.54; S, 20.46.

2.2 Solvent and devices

Recording of UV-Vis spectrum of compounds under investigation were done using a Per-kin Elmer Lambda 4B spectrophotometer by fused quartz cells of 1.0 cm length, where the spectrophotometer plots linearly the transmittance as a percentage over a

range of 500 nm (200-700) at room temperature in Acetonitrile as a polar solvent and 1,4-Dioaxne as

2.3. Computational procedure

For both accuracy and time saving, basis sets and theoretical methods are considered. Gaussian 09W program [19] was used in performing DFT computations. The DFT calculation were carried out at the B3LYP level of theory [20–22]. Ground state properties and optimized structures were obtained via the full geometry optimization using the 6-311++G(d,p) basis set [23]. Frequency calculations confirmed the stability of the optimized geometry. Gauss view 5.0 program and Chemcraft 1.8 software [24] were used to visualize geometric structures. So as to cognize the origin of the electronic spectrum, the theoretical UV-Visible spectra were calculated using the 6-311++G(d, p) basis set and the TD-DFT method in the gas phase and in solution (polar and non-polar). Polarizable Continuum Model (PCM) used for capturing gross Solvents effects. At the same theoretical level, the non-linear optical parameters were computed. Natural transition orbitals (NTOs) [25] are a good tool for scrutinizing the electronic features of the excited states for this purpose NTO were computed. Assignment of the observed electronic transitions are facilitated via computation of the natural transition orbitals (NTO's) using the Multiwfn v3.8 software package [26]. Length of charge transfer (Δr) in addition to the change of dipole moment in the ground state (ΔμCT) , due to charge transfer owing to excitations are also computed [27].

3. Results and Discussion

non-polar solvent.

3.1. Ground State Geometrical parameters

The newly synthesized rhodanine derivatives **1-5** are subjected to geometry optimization in the ground state using B3LYP/6-311++G** level of computations. C1 point group symmetry is what the optimized structure obviously belongs to. By using frequency calculations, the optimized structure of the investigated molecules was confirmed as a minimum on the potential energy surface. The optimized molecular structures, dipole moment direction and numbering system adopted in the present study are displayed in Figure 1, for the studied compounds. For the examined compounds **1–5**, a few chosen bond lengths, bond angles, and dihedral angles were enumerated together with the available X-ray experimental results as given in Table 1. The correspondence between the experimental x-ray geometric parameters and the computed values are fair [23], This may be attributed to the fact that the experimental x-ray values correspond to the solid state while the computed values pertain to the isolated molecule in the gas phase.. Majority of the calculated bond lengths show overestimation with percent ranging from 1.1 to 4.1% except C4-C5 (in **2** and **4**) and C4-O7 are underestimated with percent ranging from 0.33 to 1.39%. Generally, there is no major change. Inspection of the values of the dihedral angles compiled in Table 1, shows that almost all molecules are planar expect N3-phenyl moiety which is nearly perpendicular in all the studied compounds **1-5** with dihedral angel value 90.6˚. This would indicate the linear conjugation extended over the molecular framework except the N3-ph moiety which seems to be cross conjugated.

Table 1
Bond lengths (Å), bond angles (degrees), and dihedral angles (degrees) of the examined compounds **1–5** were estimated using optimized geometrical parameters at the B3LYP/6 311++G(d,p) theoretical scale. Figure 1,3b shows the numbering scheme

	1	**2**	**3**	**4**	**5**	**Exp***
			Bond lengths(Å)			
S1-C2	1.769	1.778	1.780	1.760	1.778	1.748
C2-N3	1.390	1.378	1.379	1.382	1.378	1.366
N3-C4	1.404	1.415	1.412	1.416	1.415	1.374
C4-C5	1.520	1.481	1.492	1.477	1.487	1.482
C5-S1	1.827	1.765	1.762	1.785	1.766	1.755
C2-S6	1.639	1.640	1.638	1.644	1.640	1.626
C4-O7	1.204	1.209	1.207	1.214	1.209	1.221
C8-N3	1.444	1.442	1.444	1.443	1.443	-
			Bond angels, degrees			
S1-C2-N3	110.4	109.8	109.8	109.2	109.7	109.8
S1-C2-S6	122.7	122.3	122.2	123.2	122.3	-
C2-N3-C4	117.9	117.4	117.4	118.1	117.5	117.9
N3-C4-O7	124.3	123.4	123.6	121.7	123.4	123.6
N3-C4-C5	111.2	109.8	110	110	110	110.6
C4-C5-S1	107.1	110.2	109.8	109	109.8	108.8
C2-S1-C5	93.2	92.5	92.8	93.4	92.8	92.9
C2-N3-C8	122	122.3	122.4	122	122.3	-
S1-C5-C19 (H19)	111.2	129.4	130.5	119.3	130.4	130.0
			Dihedral angles, degrees			
S1-C2-N3-C4	0.0	0.0	0.0	0.0	0.0	-2.5
N3-C4-C5-S1	0.0	0.0	0.0	0.0	0.0	-0.7

C2-N3-C8-C13	-90.6	-90.6	-90.6	-90.3	-90.6	-
C2-N3-C8-C9	90.6	90.6	90.6	90.6	90.6	-
S6-C2-N3-C8	0.0	0.0	0.0	0.0	0.0	-
O7-C4-N3-C8	0.0	0.0	0.0	0.0	0.0	-
C5-C4-N3-C8	179.9	179.9	179.9	179.9	179.9	-
S1-C2-N3-C8	-179.9	-179.9	-180.0	-179.9	-179.9	178.0
S1-C5-C4-O7	-179.9	-179.9	-179.9	-179.9	-180.0	178.6
S6-C2-S1-C5	-179.9	-179.9	-179.9	-179.9	-180.0	-
S1-C5-C19-C21	-	0.0	0.0	-179.8	0.0	0.8
C4-C5-C19-C21	-	-179.9	-179.9	0.1	-179.9	-
O7-C4-C5-C19	-	0.0	0.0	0.0	0.0	-
C5-C19-C21-C26	-	0.0	0.0	0.1	0.0	-
C5-C19-C21-C22	-	-179.9	-179.9	-179.9	-180.0	-179.6

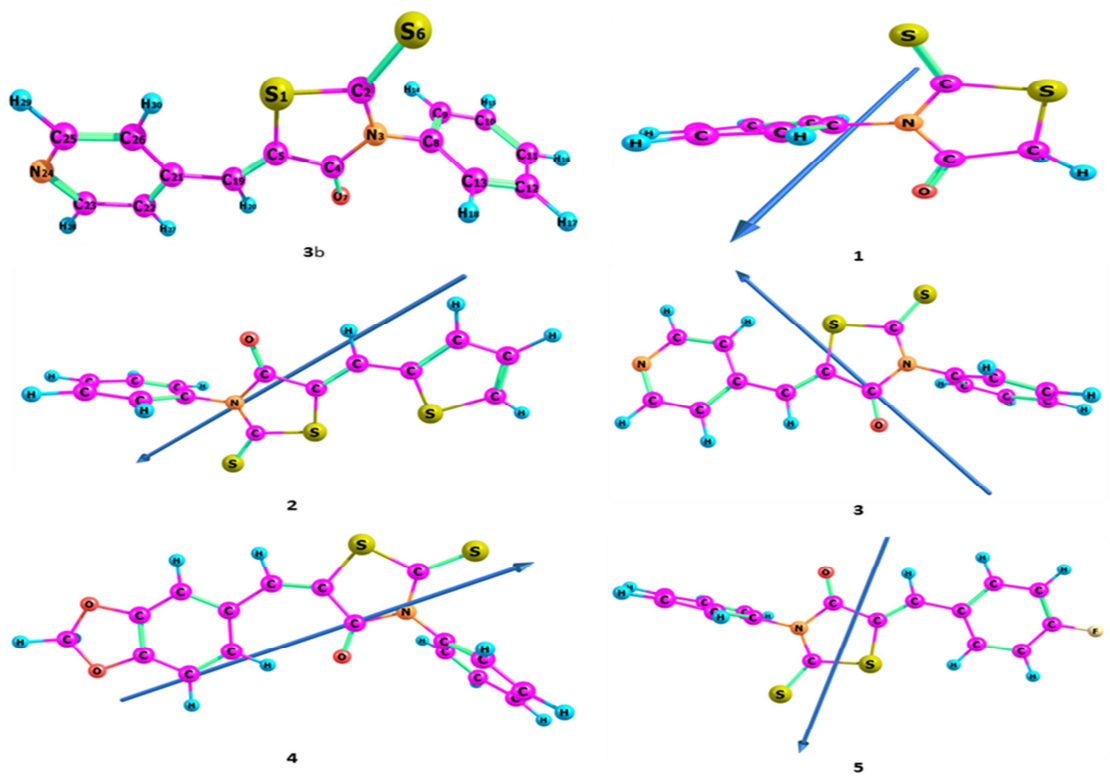

Figure 1: Numbering system (3b), optimized geometry with dipole moment vector of the of the studied compounds (**1-5**)

3.2. Quantum Global Properties

Some theoretical characteristics related to conceptual DFT have indeed been identified for the prognostication of chemical reactivity. Particularly, the global softness (S), hardness (η), then electronegativity (χ), as well as lowest unoccupied molecular orbital energy (E_{LUMO}), highest occupied molecular orbital energy (E_{HOMO}), and energy gab (E_g). The aforementioned descriptors are calculated from the optimized structure. It should be remembered that the Koopmans approximation was used to determine descriptors associated to frontier molecular orbitals with a relatively straightforward manner [28]. The molecule's sensibility to a nucleophilic attack is characterized using LUMO energy, and by way of The HOMO energy describes a molecule's susceptibility to an electrophilic attack. The system resistance for changing in the number of its electrons is inferred by global softness (S).

Electronegativity (χ) is a molecule's capacity to retain its electrons [29]. The theoretical global parameters calculated at the same level of theory are listed in Table 2. Energy gap (Eg) between HOMO and LUMO which is a gauge of electron conductivity typifies the features of molecular electrical transport and chemical stability [30]. From the data in Table 2, the order of increasing E_{HOMO} is **3 < 1 < 5 < 2 < 4** while the order of decreasing E_{LUMO} is **3 < 5 < 2 < 4 < 1**. From the order of E_{HOMO} and ELOMO it is obvious that derivative **4** holds the uppermost nucleophilicity while compound **3** has the highest electrophilicity. Analyzing the computed hardness (η) values and softness (S) values for the studied compounds revealed donor-acceptor behavior of the studied molecules, back to HOMO and LUMO energies, A tough molecule is represented by the broad energy gap, and a small energy gab represents a soft molecule. Hence, the most polarizable (softest) with easier charge transfer and highest chemical reactivity molecule is compound 4 with S=0.3117 eV, while the least polarizable molecule (hardest) is compound **1** with η=2.1722 eV. Ionization potential, I, e.V which also related to the donating properties of the molecules (the higher ionization potential value the lower the donation ability of the molecule) used to evaluate the tendency of molecules to be oxidized shows that the most probable molecule to act as reducing agent is compound **4** according to the order of ionization potential **4 < 2 < 5 < 1 < 3** ,While the order of the electron affinity values is **1 < 4 < 2** < 5 < **3** which shows that compound **1** has the highest tendency to act as oxidizing agent due to its lower value of electron affinity.

Chemical hardness and potential are among the truly essential indicators for charge transfer throughout chemical reactions and key determinants of the molecule's overall reactivity. An electron's propensity to escape is quantified via its chemical potential ω (eV), which as well correlated with their electronegativity. The probability of a molecule losing an electron grows as ω increases. Contrarily, electronegativity (χ), which measures a molecule's ability to draw electrons, demonstrates that Compounds **4** and **1** have lower electronegativity values than all other compounds under study (Table2).

Table 2
Compounds **1**–**5**'s theoretical total energy, EHOMO and ELUMO gas phase values, as well as their global reactivity descriptors, were estimated at the B3LYP/6 311++G(d,p) theorem level

	1	**2**	**3**	**4**	**5**
E_T(a.u)	-1273.7191	-1863.6989	-1558.9712	-1731.5082	-1642.2014
E_{HOMO}(a.u)	-0.23812	-0.22927	-0.24553	-0.22001	-0.23673
E_{LUMO}(a.u)	-0.07846	-0.10589	-0.11706	-0.10212	-0.10686
$E_{g.e.V}$	4.3446	3.3573	3.4958	3.2079	3.5339
$I_{e.V}$	6.4795	6.2387	6.6811	5.9867	6.4417
$A_{e.V}$	2.1350	2.8814	3.1853	2.7788	2.9078
X	4.3072	4.5600	4.9332	4.3827	4.6747
ϩ	2.1722	1.6786	1.7479	1.6039	1.7669
S	0.2301	0.2978	0.2860	0.3117	0.2829
Ω	-4.3072	-4.5600	-4.9332	-4.3827	-4.6747

3.3. Non- Quantum Global Properties

For the series of rhodanine derivatives **1-5** some physicochemical properties so called non-global descriptors are determined. The properties involved are the partitioning coefficient of water / octanol (log P), the surface area grid (SAG), moreover the molar volume (V_M), the hydration energy (HE), the molar refractivity (MR), the polarizability (Pol), and lastly the molecular weight (MW). The outputs produced by the program HyperChem 6.03 [31] are shown in Table 2. With the increase of both molecular size and weight, molar refractivity, and polarizability of the studied rhodanine derivatives relatively increase (Table 3). Hydration energy measures the degree of agonist character of a potential drug molecule. In fact, in biological environments, to create hydrogen connections between polar molecules, water particles surround them. Hydrophobic groups in rhodanine derivatives induce a hydration energy dropping off, the largest is that of the compound **4** (-10.08 kcal mol–1) and the smallest value is that of the compound **1** (-4.3 kcal mol–1). Nearly all of the investigated molecules had log P (partitioning coefficient logarithm between water and 1-octanol) values that are optimum. Values of log P should be within the range of (0 < log P < 5) for a molecule for good oral bioavailability so be able to permeate through a cell membrane. Out of this range of values the drug has low solubility (log p > 5) or has difficulty pass through the lipid membranes (log p < 0) [32]. Thus, compound **4** has the highest hydration energy whereas, compounds **1** and **5** possess the optimal values of log P.

Table 3
The examined compounds **1–5** have their non-global characteristics computed with theoretical level of B3LYP/6 311++G(d,p)

	1	**2**	**3**	**4**	**5**
Surface area $_{approx.}$	297.38	394.15	395.40	423.86	417.95
Surface area $_{grid.}$	376.36	489.94	498.32	540.08	507.00
Volume	580.42	801.08	811.22	889.88	819.64
Hydration energy $_{k.cal/mol}$	-4.38	-6.19	-7.50	-10.08	-5.82
Log p	2.22	4.83	5.16	5.22	1.3
Refractivity	58.20	82.80	81.74	89.73	97.96
Polarizability	22.85	31.40	30.44	33.49	34.06
Mass $_{a.m.u}$	209.28	303.41	298.38	341.40	315.38

3.4. Molecular Electrostatic Potential Maps

The molecular electrostatic potential (MEP) maps are correlated to the electronic density and are a highly useful signifier for elucidating electrophilic and nucleophilic reaction sites, as well as hydrogen bonding interactions and chemical activity [30]. In MEPs coloured scheme adopted in the present work is as follows, red colour matches to electron rich, moderately negative charge, that is a favourite position for electrophilic attack, blue colour stands for electron deficient, moderately positive charge that is the favourite position for nucleophilic attack. While yellow and green colour for slightly electron rich and neutral sites respectively. MEP maps were attained for investigated structures are rallied in Figure 2.

Negative areas are mostly gone over O7 atom of CO group for compounds (**1-5**) and the nitrogen atoms of pyridine group for compound **3**, while S6 atom in compound **4** is slightly red. These are the molecular residues that are most frequently targeted by electrophilic attacks. On the hand, positive regions are confined on C5 atom for **1** , C atom next to S atom on side thiophene ring for **2**, CH2 group between two O atoms on side ring for **4** making a potential site for nucleophilic attack.

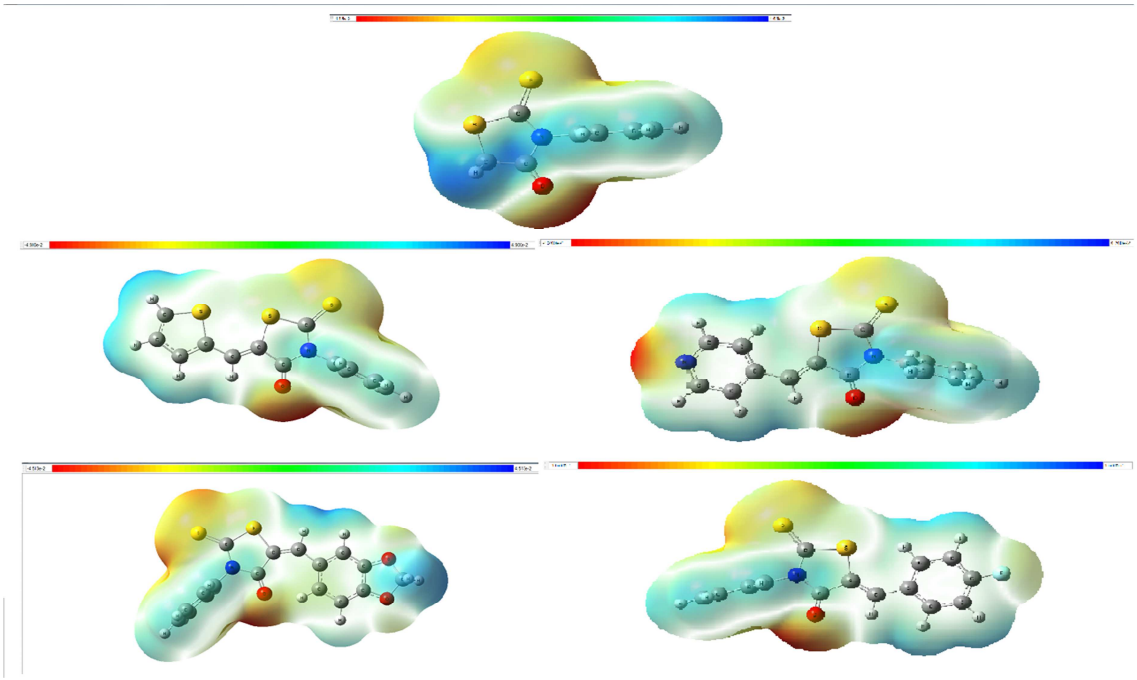

Figure 2: Molecular electrostatic potential (MEP) surface for derivatives (**1-5**)

3.5. Electronic Absorption Spectra

Through different organic solvents that 1,4-Dioxane with a dielectric constant (ε) 2.25 being a non-polar solvent then Acetonitrile with a dielectric constant (ε) 37.5 as polar solvent the experimental electronic spectra of the studied derivatives **1-5** were measured. Time-dependent DFT computations were employed to acquire the estimated electronic absorption spectrum of the optimized ground state structures of derivatives **1**–**5**, through IEFPCM to be modeled in gas phase and solvent polar and non-polar phase [30,33].

*3.5.1. Compound **1** electronic absorption spectra*

To understand the origin and type of interaction of spectral band system of the studied compounds, artificial partitioning has been made. That is, each molecule is partitioned into four subsystems as shown in Figure 3a. Four conceivable forms of interaction can occur as shown in Figure 3b. (i) with (ii) stand in for partial conjugation among Phenyl or 5-Arylmethylidene moiety with rhodanine moiety; (iii) illustrates cross conjugation wherein the phenyl ring and the two moieties do not interact; and (iv) indicate the three moieties' complete conjugation. Table 4 represents theoretical electronic absorption spectra in each subsystem along with energy gap values for each subsystem . It's clear that spectral bands in the studied compound originated from the strong partial interaction between rhodanine ring and 5-Arylmethylidene moiety, which have no relationship with the phenyl ring . The dihedral angles of the phenyl ring showed that it is out of the molecule's molecular plane (perpendicular in compounds **2**,**3**,**4** and **5**) as calculated. By inhibiting extensive conjugation with the rest of the molecule, the ≈90 degrees torsion angle of the phenyl ring, has an hyperconjugative effect over the electronic absorption spectra of the molecules under consideration.

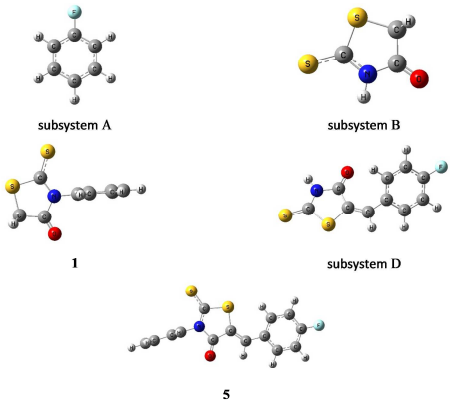

Figure 3a: The theoretical partitioning of the studied compounds into subsystems

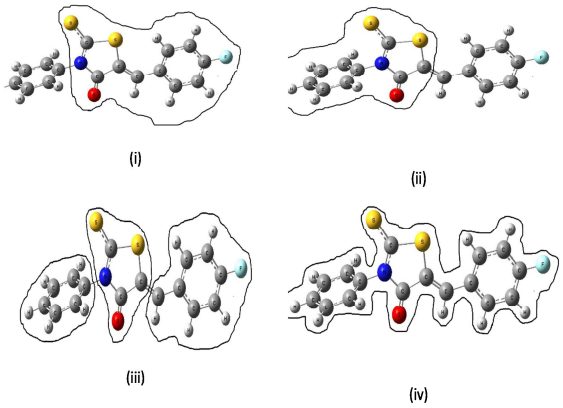

Figure 3b: The conceivable forms of interaction that can occur between the molecules many subsystems under study in this work

Table 4
Theoretical electronic absorption spectra in gas phase calculated at TD-B3LYP/6-311++G(d,p) for each subsystem along with energy gap values for each subsystem

	A	B	1	D	5
S1	178 nm	-	-	-	-
S2	-	205 nm	200 nm	-	-
S3	-	236 nm	243 nm	223 nm	227 nm
S4	-	275 nm	279 nm	278 nm	265 nm
S5	-	-	-	384 nm	370 nm
Eg,e.V	-	4.4254	4.3427	3.5232	3.5569

The spectrum of compound **5** is characterized by a new band at 370 nm while the two rhodamine bands appear at 227 and 265 nm showing a blue shift of 9 nm for S3 and 10 nm for S4. I This may be attributed to the partial linear conjugation of the 5-Arylmethylidene moiety with rhodanine ring. This type of interaction is supported by the calculated Eg values and the disappearance of the 178 nm band of para fluorobenzene in full molecule spectrum.

Table 5 compiles , for compound **1**, the experimental and calculated distinctive peak absorption wavelengths with their electronic transition configuration features such as the energy of vertical excitation, in addition to oscillator strengths (f) and the key contribution.

The theoretical and measured electronic absorption spectra of compound **1** in acetonitrile as a polar solvent and 1,4-dioxane as nonpolar solvent, in addition to the theoretical gas phase vertical excitation spectrum are displayed in Figure 5. In 1,4-dioxane the experimental spectrum consisted of two bands, the first band centered at 295 nm and the second band at 258 nm, while in acetonitrile, the first band appears at 294 nm and second one at 256 nm, respectively. All detected bands appointed π- π* transitions as unveiled from the recorded values of their molar absorptivity (ε, mol-1cm-1L). This small blue shift is attributed to changing solvent form nonpolar 1,4-dioxane to polar acetonitrile. The calculated vertical transitions of compound **1** centered at 286 nm and 247 nm respectively for1,4-dioxane and acetonitrile. The calculated bands using PCM solvation model show a blue shift by about 9 nm from the corresponding experimental values. The theoretical gas phase spectral bands are S1 (279 nm), S2 (243 nm) and S3 (199 nm).

Table 5
Compound **1** measured and computed UV spectra

	Experimental		Theoretical			
	$\lambda_{max(nm)}$	$\varepsilon_{(mol\text{-}1cm\text{-}1L)}$	λ (nm)	E(eV)	F	Major contribution
Gas phase	-	-	278	4.446	0.123	50 -> 55 -0.17112 52 -> 55 -0.10926 53 -> 55 0.65548
	-	-	243	5.093	0.152	50 -> 55 0.62401 53 -> 55 0.14180 54 -> 58 -0.24408
	-	-	199	6.223	0.122	50 -> 57 0.11093 53 -> 59 -0.10339 53 -> 62 0.10106 54 -> 63 0.59951 54 -> 64 -0.19489 54 -> 67 -0.14929
1,4-Dioxane	295	39800	286	4.334	0.199	50 -> 55 -0.1376 53 -> 55 0.67938
	258	28000	247	5.018	0.260	50 -> 55 0.67171 53 -> 55 0.12572
Acetonitrile	294.5	17200	286.66	4.325	0.182	50 -> 55 -0.13788 53 -> 55 0.67987
	256	15000	247.02	5.019	0.250	50 -> 55 0.66027 53 -> 55 0.12448 54 -> 56 0.15605

The percentage contributions of molecular parts to natural transition orbitals (NTOs) both occupied and virtual during electronic transitions among ground and singly occupied excited states for **1** achieved by PCM-B3LYP /6-311++G(d,p) level of theory are assessed with population analysis of hirshfeld shown in Table 5 in relation to these transitions. These information on the compositions of molecular orbitals is mostly centered on percent contributions of N3-phenyl and rhodanine ring linking molecular pieces to the occupied and virtual NTO's. In the first and second transitions, hirshfeld population analysis showed that the Rhodanine ring has the major contribution to both occupied (90%) and virtual NTOs (98%).

Using Multiwfn code [26], the Δr index, which measure the length of charge transfer, deviation of dipole moment of excited state with regard to ground one (ΔμCT) were computed for compounds **1-5** to study the weight of charge transfer (CT) or charge rearrangement in the course of excitations. The resulting data are listed in Table 6. When employed to distinguish amongst local excitations ($\Delta r \leq 1.5$ Å) and charge transfer excitations ($\Delta r \geq 2.0$ Å), the Δr index [27,34] may be thought of as a monitor of the length of charge transfer (CT). Concurring to Δr values, the delocalized band character of S1 and S2 transitions is clearly evident.

Table 6
Using PCM-B3LYP/6-311++G(d,p) level calculations in (1,4-dioxane and acetonitrile), hirshfeld population analysis, charge transfer length (Δr) as well as deviation in dipole moment with regard to ground state (ΔμCT) , and the percent contributions of molecular parts to natural transition orbitals for both occupied and unoccupied one in the electronic transitions of **1**

		S_0 to S_1		S_0 to S_2	
Dioxane	Δr (Å)	0.748733		0.709654	
	ΔμCT (a.u.)	1.435597		1.006241	
		NTO. Occ	NTO. Virt	NTO. Occ	NTO. Virt
	N3-ph	7.763	1.118	9.093	1.113
	Rho	92.236	98.883	90.906	98.883
	R_{gp}	-	-	-	-
Acetonitrile	Δr (Å)	0.722487		0.796997	
	ΔμCT (a.u.)	1.39233		0.677343	
		NTO. Occ	NTO. Virt	NTO. Occ	NTO. Virt
	N3-ph	9.434	1.143	9.422	1.168
	Rho	90.567	98.858	90.578	98.83
	R_{gp}	-	-	-	-

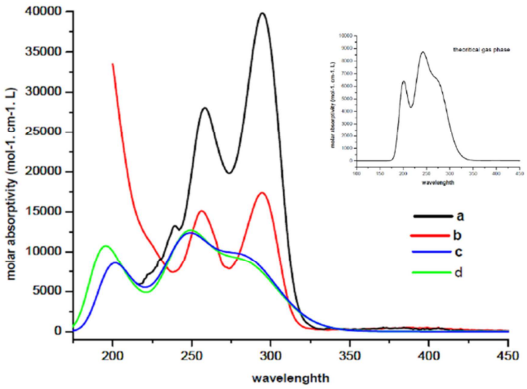

Figure 4: Theoretical and experimentally measured compound **1** absorption spectra ,where (a) experimental UV spectrum in 1,4-Dioxane, (b) experimental uv spectra in Acetonitrile , (c) 1,4-Dioxane's predicted electronic absorption spectrum and (d) theoretical electronic absorption spectra in Acetonitrile. Beside theoretical gas phase

*3.5.2. Compound **2** electronic absorption spectra*

Derivative **2** is obtained by insertion of thiophen-2-ylmethylene moiety in position 5 of **1**. The experimentally measured and theoretic spectrum for **2** in dioxane being non-polar solvent and acetonitrile being polar solvent are displayed in Figure 5 and Table 7. The thiophen-2-ylmethylene moiety led to the emergence of 399 nm new band in 1,4-Dioxane , which shows a shift by 2 nm in Acetonitrile to appear at 397 nm. In addition, the spectrum of compound **2** exhibited the two band systems characterize the spectrum of 1,the first at 293 nm shifted by 2 nm, while the second at 242 nm showed a blue shift by 16 nm from that of compound 1. On the other hand, using Acetonitrile as a solvent led to disappearance of the band at 242 nm, while the long wavelength band shows a blue shift and appears at 292 nm. The disappearance of band at 242 nm in Acetonitrile may be attributed to the low solubility of compound **2**.

Theoretically calculated spectra of **2** show that the two bands S1 and S2 are affected by solvent in different ways. Thus, while S1 is red shifted, as compared to its position in the spectrum of 1, S2 show marked blue shift. The theoretical gas phase electronic absorption spectrum exhibits S1 at 386 nm and S2 at 281 nm.

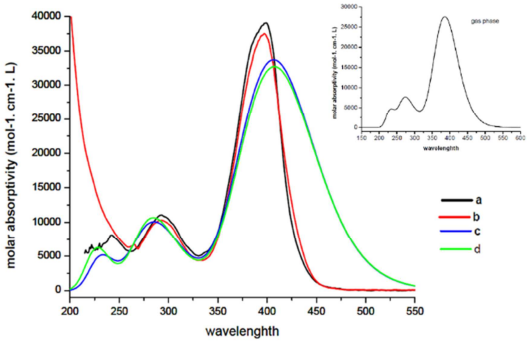

Figure 5: Theoretical and experimentally measured compound **2** absorption spectra, where (a) experimental uv spectrum in 1,4-Dioxane, (b) experimental uv spectra in Acetonitrile , (c) 1,4-Dioxane's predicted electronic absorption spectrum and (d) theoretical electronic absorption spectra in Acetonitrile. Beside theoretical gas phase

The hirshfeld population analysis data of **2** obtained at the PCM-B3LYP /6-311++G(d,p) level of calculation are listed in Table 7. These data of molecular orbital configurations basically based on the N3 phenyl, rhodanine ring and 5-Arylmethylidene (thiophen-2-ylmethylene) moieties contributions in the connection of molecular parts to the occupied and virtual NTOs.

For S1 hirshfeld population analysis showed that the rhodanine ring contributes (55%,57% ,53%,60%) whereas, the thiophen-2-ylmethylene moiety contributes (44%,41%, 46%,39%) to occupied and virtual NTO's for both solvents 1,4-dioxane and acetonitrile, respectively. This analysis indicates that S1 have a delocalized band character confirmed by charge transfer length values Δr= 0.70 Å, 0.86 Å in dioxane and acetonitrile as solvents, respectively and

deviation in dipole moment from that of ground state upon excitation ΔμCT= 1.43 a.u. , 1.39 a.u.

For the second transition, S2 , hirshfeld population analysis showed that the thiophen-2-ylmethylene moiety (65%,46%, 71%,57%) and rhodanine ring (33%,53%, 27%,41%) have the major contribution to both occupied and virtual NTO's for 1,4-dioxane and acetonitrile, respectively with Δr =1.27 Å, 1.44 Å and variation in dipole moment upon excitation= 2.36 a.u. , 1.62 a.u. to be assigned as a delocalized band.

The spectrum of compound **2** in 1,4-dioxane, shows a third transition,S3, with contribution from the N3 phenyl (61%,3%) , rhodanine ring (32%, 74%) and thiophen-2-ylmethylene moiety (5%, 22%) to both occupied and virtual NTO's. S3 is characterized by with a Δr value of 2.20 Å and large variation in dipole moment from that of ground state upon excitation ΔμCT= 5.28 a.u. these data clearly indicate the charge transfer character of S3 , in which the transfer occurs to the rhodanine ring and thiophen-2-ylmethylene moiety from N3 phenyl group (c.f. Figure 6 ,Table 8)

Table 7
Compound **2** measured and computed UV spectra, at TD-B3LYP/6-311++G (d,p)

	Experimental		Theoretical				
	$\lambda_{max(nm)}$	$\varepsilon_{(mol\text{-}1cm\text{-}1L)}$	λ(nm)	E(eV)	F	Major contribution	
Gaseous phase	-	-	386	3.213	0.680	78 -> 79	0.70227
	-	-	281	4.405	0.044	72 -> 79	0.51117
						73 -> 79	0.10450
						75 -> 79	-0.12854
						76 -> 79	-0.17271
						78 -> 80	-0.39685
1,4-Dioxane	399	39000	406	3.048	0.832	78 -> 79	0.70402
	293	11000	277	4.468	0.112	72 -> 79	0.46479
						73 -> 79	-0.21445
						75 -> 79	0.14166
						76 -> 79	0.18085
						78 -> 80	0.39280
	242	8000	234	5.300	0.050	75 -> 80	-0.15638
						76 -> 80	0.61153
						77 -> 83	-0.24651
						78 -> 84	0.12578
Acetonitrile	397	37400	407	3.042	0.807	78 -> 79	0.70359
	292.5	10200	279	4.438	0.138	72 -> 79	-0.25859
						73 -> 79	-0.38419
						76 -> 79	0.19905
						78 -> 80	0.46742

Table 8
Using PCM-B3LYP/6-311++G(d,p) level calculations in (1,4-dioxane and acetonitrile), hirshfeld population analysis was used to discern charge transfer length (Δr), deviation in dipole moment with regard to ground state (ΔμCT) , and the fraction contributions of molecular parts to (NTOs) in transitions of **2**

		S_0 to S_1		S_0 to S_2		S_0 to S_3	
Dioxane	Δr (Å)	0.706673		1.270193		2.204287	
	ΔμCT (a.u.)	1.323862		2.364128		5.288157	
		NTO. Occ	NTO. Virt	NTO. Occ	NTO. Virt	NTO. Occ	NTO. Virt
	N3-ph	0.533	0.378	1.197	0.34	61.361	3.235
	Rho	55.454	57.868	33.59	53.352	32.663	74.55
	R_{gp}	44.017	41.753	65.214	46.309	5.978	22.216
Acetonitrile	Δr (Å)	0.863433		1.449238		-	
	ΔμCT (a.u.)	1.615485		1.620239		-	
	NTO pop.	NTO. Occ	NTO. Virt	NTO. Occ	NTO. Virt	NTO. Occ	NTO. Virt
	N3-ph	0.453	0.422	1.386	0.928	-	-
	Rho	53.268	60.103	27.023	41.412	-	-
	R_{gp}	46.28	39.475	71.589	57.659	-	-

Transition state	S_0 to S_1		S_0 to S_2		S_0 to S_3	
Solvent	NTO. Occ	NTO. Virt	NTO. Occ	NTO. Virt	NTO. Occ	NTO. Virt
Dioxane	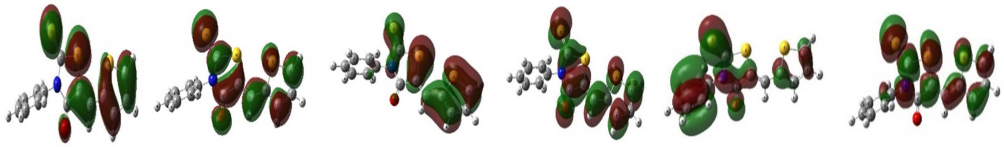					
Acetonitrile	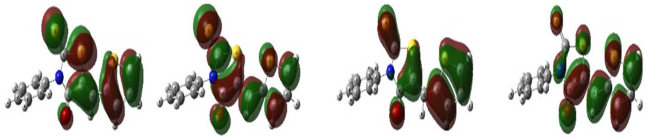				-	-

Figure 6: Using hirshfeld population analysis, Compound **2** natural transition orbitals of transitions calculated at the PCM-B3LYP/6-311++G (d,p) level of theory for both solvents

*3.5.3. Compound **3** absorption spectra*

Compound **3** is obtained by introducing pyridin-4-ylmethylene moiety in position 5 of **1**. The experimentally measured and theoretic spectra of derivative **3** in dioxane being non-polar solvent and acetonitrile being polar solvent are displayed in Figure 7 and Supplementary Table 2.The insertion of pyridin-4-ylmethylene moiety led to appearance of a new band in the experimental spectra at 366 nm. Solvent polarity has no effect on the position of this band however, the 366 band is of much higher molar absorptivity in 1,4-Dioxane. The spectrum of compound 3 in acetonitrile, exhibits two more bands at exhibited two bands in Acetonitrile, first at 282.5 nm and the second at 255 nm. Changing solvent to dioxane lead to the disappearance of the long wavelength band at 295 nm of compound **1**, while the second band show a red shift by 16 nm to appear at 259 nm. The theoretically gas phase computed electronic absorption bands are in good agreement with the experimentally observed bands. This spectrum is sensitive to solvent polarity, however, where the first high valued wavelength band shows a red shift by 16 nm in dioxane and by 15 nm in acetonitrile, S2 have a blue shift by 17.5 nm in Acetonitrile and S3 show a red shift by 16 nm in 1,4-Dioxane and by 5 nm in Acetonitrile. The theoretical gas phase electronic absorption spectra exhibit three excited states S1 at 366 nm, which is identical to that band observed experimentally in both solvents, S2 at 254 nm and S3 at 227 nm.

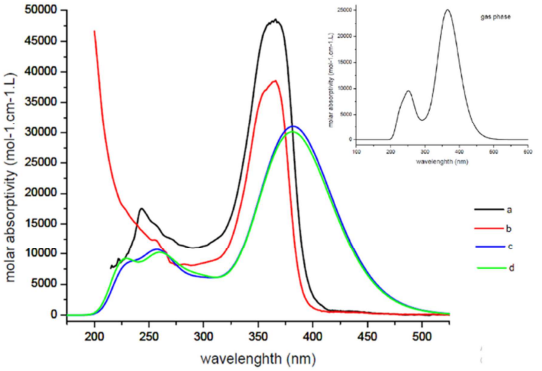

Figure 7: Theoretical and experimentally measured compound **3** absorption spectra, where (a) represents experimental uv spectrum in 1,4-Dioxane, (b) represents experimental uv spectra in Acetonitrile , (c) 1,4-Dioxane's predicted electronic absorption spectrum, and (d) represents theoretical electronic absorption spectra in Acetonitrile. Beside theoretical gas phase

Supplementary Table 3 compiles the hirshfeld population analysis data of compound **3** calculated at PCM-B3LYP/6-311G++ (d,p) level of theory. This analysis is based on the percent contributions of the N3 phenyl, the Rhodanine ring and the 5-Arylmethylidene (pyridin-4-ylmethylene) molecular parts to NTOs the occupied and virtual.

Applying hirshfeld population analysis to the first transition, reviles that the rhodanine ring contributes (67%, 57%) whereas the pyridin-4-ylmethylene moiety contributes (31%, 41%) to the occupied and virtual NTO's, respectively. Solvent polarity has no effect on these percent contributions. This transition is delocalized as it is evident from the Δr value (< 2.0 Å) and dipole moment change upon excitation $\Delta\mu CT$ of 1.66 a.u. ,and 1.88 a.u. for the two moieties respectively.

For the second transition, the hirshfeld population analysis showed that the rhodanine ring (45%, 59%) and pyridin-4-ylmethylene (52%, 40%) have the

major contributions to both occupied and virtual NTO's for 1,4-dioxane with Δr =1.0 Å and variation in dipole moment upon excitation= 2.0 a.u. to be assigned as a delocalized band, while in acetonitrile, hirshfeld population analysis showed that the rhodanine ring (88%) have the major contribution to occupied NTO and whereas, the pyridin-4-ylmethylene (44%) and the rhodanine ring (55%) contributes considerably to virtual NTO revealing a charge transfer from rhodanine to pyridin-4-ylmethylene moiety which is confirmed by the 2.0 Å Δr value and large alteration in dipole moment after excitation (4.05 a.u.) uncovering a major deformation in excited state geometry from that of the ground state and this band assigned as charge transfer band .

Compound **3** shows a third transition in acetonitrile also with major contribution of rhodanine ring (65%, 57%) and pyridin-4-ylmethylene (32%, 42%) to both occupied and virtual NTO's with Δr= 1.02 Å and ΔμCT= 1.91 a.u. indicating its delocalized band character.

*3.5.4. Compound **4** electronic absorption spectra*

Compound **4** is obtained by insertion of Benzo[d][1,3]dioxol-5-ylmethylene moiety in position 5 of **1**. The experimentally measured and theoretic spectra of derivative **4** in dioxane being non-polar solvent and acetonitrile as a polar solvent are displayed in Figure 8 and the corresponding data are compiled in Supplementary Table 4. The insertion of Benzo[d][1,3]dioxol-5-ylmethylene moiety led to appearance of two new bands in the experimental spectra centered at 404 nm and 242 nm in 1,4-Dioxane; both are sensitive to solvent polarity. Thus, while the first band suffers a slight blue shift (5 nm) to appear at 399 nm in Acetonitrile with much higher molar absorptivity. The second band vanished in Acetonitrile. The spectrum of compound **4** exhibited the remaining two bands centered at 292 nm and 259 nm. These two bands correspond very well to those observed in the case of compound **1**. Solvent polarity has but a slight effect on these two bands.

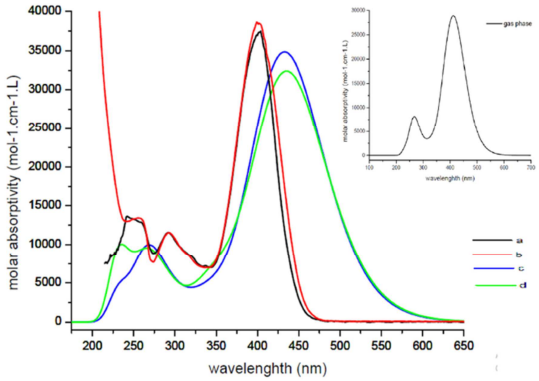

Figure 8: Theoretical and experimentally measured compound **4** absorption spectra, where (a) experimental uv spectrum in 1,4-Dioxane, (b) experimental uv spectra in Acetonitrile , (c) 1,4-Dioxane's predicted electronic absorption spectrum, and (d) theoretical electronic absorption spectra in Acetonitrile. beside theoretical gas phase

The theoretical electronic absorption spectrum computed for compound **4** predicts the 4-band system yet the position of all bands is red shifted as compared to the corresponding experimental values. The first band is the most affected. have a red shift in all existed states, S1 by 29 nm ,S2 by 1 nm , S3 by 7 nm and S4 by 6 nm for that of 1,4-Dioxane, while the calculated for Acetonitrile, also show a red shift for S1 by 37 nm, for S2 by 3.5 nm and for S3 by 10 nm. The theoretical gas phase electronic absorption spectra predicted to electronic transitions S1 at 412 nm and S2 at 265 nm.

Regarding N3 phenyl, Rhodanine ring and 5-Arylmethylidene (Benzo[d][1,3]dioxol-5-ylmethylene) moieties contributions to connection of the molecular parts to the occupied and virtual NTO's hirshfeld population analysis results calculated at the PCM-B3LYP/6-311++G(d,p) level of computation are tabulated in Supplementary Table 5.

Examining The first transition, hirshfeld population analysis showed that Benzo[d][1,3]dioxol-5-ylmethylene moiety (60%,42%, 65%,41%) and rhodanine ring (39%,56%, 34%, 57%) have the major contribution to both occupied and virtual NTO's for 1,4-dioxane and acetonitrile respectively with Δr less than 2.0 Å and deviation of dipole moment with regard to ground state ΔμCT 2.60 a.u. ,3.49 a.u. to be assigned as a delocalized band.

The second transition, hirshfeld population analysis showed that Benzo[d][1,3]dioxol-5-ylmethylene moiety (86%,55%, 74%,48%) and rhodanine ring (11%,43%, 22%,51%) have the major contribution to both occupied and virtual NTO's for 1,4-dioxane and acetonitrile respectively with Δr

=2.11 Å, 2.14 Å and variation in dipole moment upon excitation= 3.83 a.u. , 4.33 a.u. to be clearly assigned as a CT band.

The third transition, hirshfeld population analysis showed that Benzo[d][1,3]dioxol-5-ylmethylene moiety (62%,98%, 67%,98%) and rhodanine ring (37%,1%, 31%,1%) have the major contribution to both occupied and virtual NTO's for 1,4-dioxane and acetonitrile respectively with Δr =2.19 Å, 2.01 Å and variation in dipole moment upon excitation= 2.09 a.u. , 1.46 a.u. to be clearly assigned as a charge transfer band, where the charge transfer occur to Benzo[d][1,3]dioxol-5-ylmethylene moiety(98% virt. NTO) from rhodanine ring.

Compound **4** shows a fourth transition in 1,4-dioxane with major contribution of Benzo [d][1,3]dioxol-5-ylmethylene moiety(59%,13%) and rhodanine ring (37%, 83%) to both occupied and virtual NTO's with Δr= 3.23 Å and ΔμCT= 5.38 a.u. which obviously indicate charge transfer from Benzo[d][1,3]dioxol-5-ylmethylene moiety to rhodanine ring.

*3.5.5. Compound **5** electronic absorption spectra*

Derivative **5** is obtained by insertion of 4-Fluorobenzylidene moiety in position 5 of **1**. The experimentally measured and theoretic absorption spectra of compound **5** in dioxane and acetonitrile as solvents are displayed in Figure 9 and Supplementary Table 6. The introduction of 4-Fluorobenzylidene moiety led to the appearance of a new band at 378 nm in 1,4-Dioxane, this band is slightly blue shifted to appear at 376 nm in Acetonitrile with almost equal molar absorptivity. Compound **5** exhibited the remaining two bands in 1,4-Dioxane at 275.5 nm and at 242 nm, the two bands are blue shifted as compared to the corresponding bands of compound 1,the first by 19.5 nm and the second by 16 nm. Increasing solvent polarity (Acetonitrile) almost cause no change in the position of first band (275 nm) but led to a red shift in the second by 24 nm to appear at 266 nm. The theoretical electronic absorption spectrum of compound **5** is in good harmony with the experimentally observed one. The gross solvent effect captured by the PCM model indicates that the computed gas phase transitions are solvent dependent.

The data obtained from hirshfeld population analysis for electronic transitions of compound **5** are listed in Supplementary Table 7. These data of molecule orbital arrangements are fundamentally related to N3 phenyl, Rhodanine ring and 5-Arylmethylidene (4-Fluorobenzylidene) moieties involvement to molecular parts connection to the occupied and virtual NTO's.

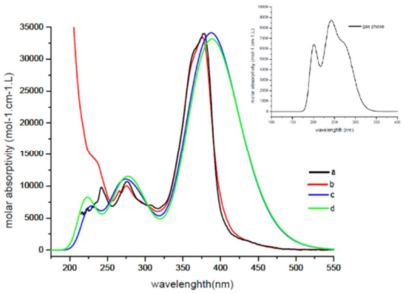

Figure 9: Theoretical and experimental electronic absorption spectra of compound **5**,where (a) experimental uv spectrum in 1,4-Dioxane, (b) experimental uv spectra in Acetonitrile , (c) 1,4-Dioxane's predicted electronic absorption spectrum, and (d) theoretical electronic absorption spectra in Acetonitrile. beside theoretical gas phase

For the first transition, hirshfeld population analysis showed that rhodanine ring (59%,61%, 57%, 63%) and 4-Fluorobenzylidene moiety (40%,37%, 41%,36%) have the major contributions to both occupied and virtual NTO's for 1,4-dioxane and acetonitrile respectively with charge transfer length Δr 0.79 Å, 0.90 Å and deviation of dipole moment with regard to ground state ΔμCT 1.48 a.u. ,1.70 a.u. to be assigned as a delocalized band.

For the second transition, hirshfeld population analysis showed that rhodanine ring (56%,74%, 55%, 72%) and 4-Fluorobenzylidene moiety (42%,22%, 43%,24%)have the major contributions to both occupied and virtual NTO's for 1,4-dioxane and acetonitrile respectively with Δr =1.43 Å, 1.52 Å and variation in dipole moment upon excitation= 1.93 a.u. , 1.03 a.u. These Δr values, suggest the delocalized nature of this band .

For the third transition, hirshfeld population analysis showed that N3 phenyl (75%,3%), rhodanine ring (18%, 73%) and 4-Fluorobenzylidene moiety (5%, 23%) have contributed to both occupied and virtual NTO's for 1,4-dioxane with the large charge transfer length Δr =3.44 Å besides large deviation of dipole moment from ground state upon excitation= 6.29 a.u. to be described as a charge transfer band where the charge transfer migrates to the rhodanine ring and 4-Fluorobenzylidene moiety, while in acetonitrile Hirshfeld population analysis showed that the rhodanine ring (57%,2%) and 4-Fluorobenzylidene moiety (42%, 97%) have the major contributions to both occupied and virtual NTO's reviling a charge transfer from rhodanine to 4-Fluorobenzylidene moiety which is confirmed by 3.31 Å Δr value and large change in dipole moment upon excitation (3.60 a.u.) to be ascribed as a charge transfer band in which the transfer occur to 4-Fluorobenzylidene moiety which has the major contribution to virt. NTO (97%).

4. Conclusions

Electronic structure, ultraviolet electronic absorption spectra , and the global reactivity descriptors of some newly synthesized rhodanine derivatives **1-5** are experimentally and theoretically investigated via using B3LYP functional and 6-311++G(d,p) basis set. From the calculated data of HOMO and LUMO energy, the order of increasing E_{HOMO} is **3 < 1 < 5 < 2 < 4** while the order of decreasing E_{LUMO} is **3 < 5 < 2 < 4 < 1.** From the order of E_{HOMO} and E_{LOMO} compound **4** has the highest nucleophilicity while compound **3** has the highest electrophilicity. Also from the global descriptors, the polarizable (softest) with easier charge transfer and highest chemical reactivity molecule is compound **4** with S=0.3117 eV, while the least polarizable molecule (hardest) is compound **1** with η=2.1722 eV. The most probable molecule to act as reducing agent is compound **4** according to the order of ionization potential **4 < 2 < 5 < 1 < 3**, while the order of the electron affinity values is **1 < 4 < 2 < 5 < 3** which shows that compound **1** has the highest tendency to act as oxidizing agent. The electronic absorption spectra of the studied rhodanines **1-5** were scanned, in polar and nonpolar solvents, and are modelled theoretically employing high-level quantum mechanical techniques and implicit solvation in the gas phase and aqueous solution. The distribution of the charge and assignment of the observed and computed transitions are carried out. The sub-systematization of all the analysed derivatives reveals the origin of each absorption band. Furthermore, NTO's were computed in order to determine the participation percentage of molecular moieties in the respective electronic transitions.

5. Conflicts of interest

The authors state that they have no competing interests to disclose.

6. Formatting of funding sources

Funding institutions from the public, commercial, and non-profit sectors did not award any specific grants for this research.

7. Acknowledgments

Authors are grateful to Professor Hamdi Hassanien and his research group for making the rhodanines studied in the present work, available.

8. References

1. Jiachun Liu, Y.W.H.P.X.Z.W.Z.Y.W. and M.L. A Comprehensive Review on the Biological and Pharmacological Activities of Rhodanine Based Compounds for Research and Development of Drugs. *Med. Chem.* **2018**, *18*, 948–961, doi:10.2174/1389557516666160928162724.
2. Paladhi, S.; Jana, B.; Pathak, S.; Manna, S.K. Nucleophilic Rhodanine, Thiazolidine-2,4-Dione and Thiazol-4(5H)-One Substrates in Asymmetric Reactions. *Arkivoc* **2019**, *2019*, 256–292, doi:10.24820/ark.5550190.p010.911.
3. Kaur Manjal, S.; Kaur, R.; Bhatia, R.; Kumar, K.; Singh, V.; Shankar, R.; Kaur, R.; Rawal, R.K. Synthetic and Medicinal Perspective of Thiazolidinones: A Review. *Bioorg. Chem.* **2017**, *75*, 406–423, doi:10.1016/j.bioorg.2017.10.014.
4. Trotsko, N.; Kosikowska, U.; Paneth, A.; Wujec, M.; Malm, A. Synthesis and Antibacterial Activity of New (2,4-Dioxothiazolidin-5-Yl/Ylidene)Acetic Acid Derivatives with Thiazolidine-2,4-Dione, Rhodanine and 2-Thiohydantoin Moieties. *Saudi Pharm. J.* **2018**, *26*, 568–577, doi:10.1016/j.jsps.2018.01.016.
5. Koppireddi, S.; Komsani, J.R.; Avula, S.; Pombala, S.; Vasamsetti, S.; Kotamraju, S.; Yadla, R. Novel 2-(2,4-Dioxo-1,3-Thiazolidin-5-Yl)Acetamides as Antioxidant and/or Anti-Inflammatory Compounds. *Eur. J. Med. Chem.* **2013**, *66*, 305–313, doi:10.1016/j.ejmech.2013.06.005.
6. Barros, C.D.; Amato, A.A.; Oliveira, T.B. de; Iannini, K.B.R.; Silva, A.L. da; Silva, T.G. da; Leite, E.S.; Hernandes, M.Z.; Lima, M. do C.A. de; Galdino, S.L.; et al. Synthesis and Anti-Inflammatory Activity of New Arylidene-Thiazolidine-2,4-Diones as PPARγ Ligands. *Bioorg. Med. Chem.* **2010**, *18*, 3805–3811, doi:10.1016/j.bmc.2010.04.045.
7. Liu, X.-F.; Zheng, C.-J.; Sun, L.-P.; Liu, X.-K.; Piao, H.-R. Synthesis of New Chalcone Derivatives Bearing 2,4-Thiazolidinedione and Benzoic Acid Moieties as Potential Anti-Bacterial Agents. *Eur. J. Med. Chem.* **2011**, *46*, 3469–3473, doi:10.1016/j.ejmech.2011.05.012.
8. Aneja, D.K.; Lohan, P.; Arora, S.; Sharma, C.; Aneja, K.R.; Prakash, O. Synthesis of New Pyrazolyl-2, 4-Thiazolidinediones as Antibacterial and Antifungal Agents. *Org. Med. Chem. Lett.* **2011**, *1*, 15, doi:10.1186/2191-2858-1-15.
9. Purohit, S.S.; Alman, A.A.; Shewale, J. SYNTHESIS & ANTIMICROBIAL ACTIVITY OF A NEW SERIES OF 3, 5-DISUBSTITUTED THIAZOLIDINE-2, 4-DIONES.; 2012.
10. Marc, G.; Ionuț, I.; Pîrnău, A.; Vlase, L.; Cristian Vodnar, D.; Duma, M.; Tiperciuc, B.; Oniga, O. *MICROWAVE ASSISTED SYNTHESIS OF 3,5-DISUBSTITUTED THIAZOLIDINE-2,4-DIONES WITH ANTIFUNGAL ACTIVITY. DESIGN, SYNTHESIS, VIRTUAL AND IN VITRO ANTIFUNGAL SCREENING*; 2017; Vol. 65;.
11. Tomašić, T.; Peterlin Mašič, L. Rhodanine as a Scaffold in Drug Discovery: A Critical Review of Its Biological Activities and Mechanisms of Target Modulation. *Expert Opin. Drug Discov.* **2012**, *7*, 549–560, doi:10.1517/17460441.2012.688743.
12. Patel, A.B.; Kumari, P. Recent Advances in the Biological Importance of Rhodanine Derivatives. In *Scope of Selective Heterocycles from Organic and Pharmaceutical Perspective*; InTech, 2016.
13. Mendgen, T.; Steuer, C.; Klein, C.D. Privileged Scaffolds or Promiscuous Binders: A

Comparative Study on Rhodanines and Related Heterocycles in Medicinal Chemistry. *J. Med. Chem.* **2012**, *55*, 743–753, doi:10.1021/jm201243p.
14. Bhatti, R.S.; Shah, S.; Suresh; Krishan, P.; Sandhu, J.S. Recent Pharmacological Developments on Rhodanines and 2,4-Thiazolidinediones. *Int. J. Med. Chem.* **2013**, *2013*, 1–16, doi:10.1155/2013/793260.
15. Allan, F.J.; Allan, G.G.; Crank, G.; Jack, J. The Condensation of Rhodanine and Derivatives with Benzaldehyde Sulphonic Acids. *Recl. des Trav. Chim. des Pays-Bas* **2010**, *79*, 247–254, doi:10.1002/recl.19600790304.
16. Tomasic, T.; Masic, L.P. Rhodanine as a Privileged Scaffold in Drug Discovery. *Curr. Med. Chem.* **2009**, *16*, 1596–1629.
17. Khaled, D.M.; Elshakre, M.E.; Noamaan, M.A.; Butt, H.; Abdel Fattah, M.M.; Gaber, D.A. A Computational QSAR, Molecular Docking and In Vitro Cytotoxicity Study of Novel Thiouracil-Based Drugs with Anticancer Activity against Human-DNA Topoisomerase II. *Int. J. Mol. Sci.* **2022**, *23*, doi:10.3390/ijms231911799.
18. Andreasch, R.; Zipser, A. Über Substituierte Rhodaninsäuren Und Ihre Aldehydkondensationsprodukte. *Monatshefte für Chemie und verwandte Teile anderer Wissenschaften* **1903**, *24*, 499–518, doi:10.1007/BF01525850.
19. M. J. Frisch, G.; Trucks, W.; Schlegel, H.B..; Scuseria, G.E..; Robb, M.A..; Cheeseman, J.R.; Scalmani, G.; Barone, V..; Mennucci, B..; Petersson, G.A.; et al. Gaussian 09, Revision E. 01; Gaussian. *Gaussian, Inc. Wallingford, CT* **2009**.
20. Lee, C.; Yang, W.; Parr, R.G. Development of the Colle-Salvetti Correlation-Energy Formula into a Functional of the Electron Density. *Phys. Rev. B* **1988**, *37*, 785–789, doi:10.1103/PhysRevB.37.785.
21. Becke, A.D. Density-functional Thermochemistry. III. The Role of Exact Exchange. *J. Chem. Phys.* **1993**, *98*, 5648–5652, doi:10.1063/1.464913.
22. Calais, J.-L. Density-Functional Theory of Atoms and Molecules. R.G. Parr and W. Yang, Oxford University Press, New York, Oxford, 1989. IX + 333 Pp. Price £45.00. *Int. J. Quantum Chem.* **1993**, *47*, 101–101, doi:10.1002/qua.560470107.
23. Anbarasan, R.; Dhandapani, A.; Manivarman, S.; Subashchandrabose, S.; Saleem, H. Synthesis and Spectroscopical Study of Rhodanine Derivative Using DFT Approaches. *Spectrochim. Acta - Part A Mol. Biomol. Spectrosc.* **2015**, *146*, 261–272, doi:10.1016/j.saa.2015.02.097.
24. Zhurko, G.A.; Zhurko, D.A. ChemCraft-Graphical Program for Visualization of Quantum Chemistry Computations. *Chemcr. v1.8.* **2020**.
25. Martin, R.L. NATURAL TRANSITION ORBITALS. *J. Chem. Phys.* **2003**, *118*, 4775–4777.
26. Analyzer, A.M.W.; Lu, T. Multiwfn. In *Software Manual*; 2021.
27. Guido, C.A.; Cortona, P.; Mennucci, B.; Adamo, C. On the Metric of Charge Transfer Molecular Excitations: A Simple Chemical Descriptor. *J. Chem. Theory Comput.* **2013**, doi:10.1021/ct400337e.
28. Koopmans, T. Über Die Zuordnung von Wellenfunktionen Und Eigenwerten Zu Den Einzelnen Elektronen Eines Atoms. *Physica* **1934**, *1*, 104–113, doi:10.1016/S0031-8914(34)90011-2.
29. Moustafa, H.; Elshakre, M.E.; Elramly, S. Electronic Structure and Nonlinear Optical Properties (NLO) of 2,4-Di-Aryl-1,5-Benzothiazepine Derivatives Using DFT Approach. *J. Mol. Struct.* **2017**, *1136*, 25–36, doi:10.1016/j.molstruc.2017.01.070.
30. Moustafa, H.; Moussa, A.Z.; Elshakre, M.E.; Hassaneen, H.M.E. DFT, Electronic Absorption Spectra and Non-Linear Optical Properties of Some 4H-Benzo[h]Chromene Derivatives. Solvent Effect and TD-DFT Approach. *Egypt. J. Chem.* **2021**, doi:10.21608/ejchem.2021.69996.3544.
31. Laxmi, D.; Priyadarshy, S. HyperChem 6.03. *Biotech Softw. Internet Rep.* **2002**, doi:10.1089/152791602317250351.
32. Abdel-Rahman, L.H.; El-Khatib, R.M.; Abdel-Fatah, S.M.; Moustafa, H.; Alsalme, A.M.; Nafady, A. Novel Cr (III), Fe (III) and Ru (III) Vanillin Based Metallo-Pharmaceuticals for Cancer and Inflammation Treatment: Experimental and Theoretical Studies. *Appl. Organomet. Chem.* **2019**, doi:10.1002/aoc.5177.
33. El-Taher, S.; Metwaly, M. DFT and PCM-TD-DFT Investigation of the Electronic Structures and Spectra of 5-(3-Phenyl-2-Propenylidene)-2-Thioxo-4-Thiazolidinone Derivatives. *J. Mol. Struct.* **2017**, doi:10.1016/j.molstruc.2017.01.014.
34. Abdel-Rahman, L.H.; Al–Farhan, B.S.; Al Zamil, N.O.; Noamaan, M.A.; El-Sayed Ahmed, H.; Adam, M.S.S. Synthesis, Spectral Characterization, DFT Calculations, Pharmacological Studies, CT-DNA Binding and Molecular Docking of Potential N, O-Multidentate Chelating Ligand and Its VO(II), Zn(II) and ZrO(II) Chelates. *Bioorg. Chem.* **2021**, doi:10.1016/j.bioorg.2021.105106.